JOURNAL OF SPACECRAFT AND ROCKETS
Vol. 45, No. 2, March–April 2008

Improved Aerodynamics for Configurations with Boattails

F. G. Moore* and L. Y. Moore†
Aeroprediction, Inc., King George, Virginia 22485

DOI: 10.2514/1.29687

Aeroprediction, Incorporated undertook a review of the 2005 version of the Aeroprediction Code (AP05) when applied to configurations with boattails. It was found the code gave poor results for roll and pitch damping for configurations with long boattails (boattails greater than about 1 caliber in length). It was found that center of pressure predictions needed improvement as well. As a result, several improved methods were developed and implemented into the AP05 which will be released in 2009 as the AP09. Comparison of the new methods to experimental data for projectiles, mortars, and low-drag bombs showed significant improvement in roll and pitch damping predictions, as well as improvement in normal force and center of pressure.

Nomenclature

A_{ref}	=	reference area, maximum cross-sectional area of body, if a body is present, or planform area of wing, if wing alone), ft^2
AR	=	aspect ratio
b	=	wing span (not including body), ft
C_A	=	axial force coefficient
C_{A_B}, C_{A_F}, C_{A_W}	=	base, skin friction, and wave components, respectively, of axial force coefficient
C_{A_0}	=	axial force coefficient at 0 deg angle of attack
C_{ℓ_p}	=	roll damping moment coefficient
C_M	=	pitching moment coefficient, based on reference area and body diameter, if body present, or mean aerodynamic chord, if wing alone
C_{M_B}, C_{M_T}	=	pitching moment coefficient of body or tail alone, respectively
$C_{M_q} + C_{M_\alpha}$	=	pitch damping moment coefficient $\lfloor C_M(q)/(qd/2V_\infty) + C_M(\dot{\alpha})/(\dot{\alpha}d/2V_\infty)\rfloor$
C_{M_α}	=	pitching moment coefficient derivative, per radian
C_N	=	normal-force coefficient
C_{N_B}	=	normal-force coefficient of body alone
C_{N_α}, $(C_{N_\alpha})_{n,a,b}$	=	total normal-force coefficient derivative, per radian, and normal-force coefficient derivative of nose, afterbody, or boattail, respectively
C_P	=	pressure coefficient $P - P_\infty/\frac{1}{2}\rho_\infty V_\infty^2$
c, c_r, c_t	=	local chord, root, and tip chord, respectively
c.g.	=	center of gravity location, cal, ft, or in.
d_B	=	body base diameter, ft
d_N	=	diameter of truncated nose tip, ft
d_{ref}	=	reference body diameter, ft
F_6, F_8	=	empirical factors used to represent aerodynamics of six and eight fins based on four fin aerodynamics
ℓ, ℓ_n, ℓ_a, ℓ_B	=	total body, nose, afterbody, or boattail length, respectively, ft or cal
M_∞	=	freestream Mach number
P_L, P_∞	=	local and freestream pressure, respectively, lb/ft^2
p, q	=	roll and pitch rate, respectively, rad/s
Q_L, Q_∞	=	local or freestream dynamic pressure, lb/ft^2
r_B, r_W	=	local body radius and body radius at wing, respectively, ft
r_r	=	reference body radius, ft
$X_{\text{c.g.}}$	=	distance to center of gravity, ft
$X_{\text{c.p.}}$, $(X_{\text{c.p.}})_{n,a,b}$	=	center of pressure (in ft or cal from some reference point that can be specified) in x direction or center of pressure of a body component, respectively
$X_{\text{c.p.}}/d$	=	center of pressure (cal from some reference point)
X_{LE}, X_{AFT}	=	distance from nose tip to wing leading edge or afterbody
α	=	angle of attack, deg
δ^*	=	boundary-layer displacement thickness, ft
θ_b	=	boattail angle, deg
Φ	=	roll position of missile fins [$\Phi = 0$ deg corresponds to fins in the plus (+) orientation, $\Phi = 45$ deg corresponds to fins rolled to the cross (×) orientation].

Presented at the Atmospheric Flight Mechanics Conference, Hilton Head Island, SC, 1 August 2007; received 31 March 2007; revision received 25 July 2007; accepted for publication 4 August 2007.

*President, 9449 Grover Drive, Suite 201; drfgmoore@hotmail.com. Associate Fellow AIAA.
†Computer Scientist.

Introduction

A COUPLE of years ago, Aeroprediction, Inc. (API) was providing aerodynamic support to the Naval Surface Warfare Center, Dahlgren Division (NSWCDD) on a mortar round. API calculated normal force, axial force, pitching moment, center of pressure, roll, and pitch damping moments for a wide variety of Mach numbers and angles of attack for several different mortar configurations. After the aerodynamic computations were complete, a set of experimental data on one of the configurations was made available to API. In comparing the AP05 [1] predictions to experimental data, it was obvious that a large boundary layer was present on the long boattail of the mortar, negating some of the fin effectiveness in providing static stability along with reducing roll and pitch damping.

During the last two years, API undertook an evaluation of the weak areas of the Aeroprediction Code (AP05) when used on weapons with boattails, as well as developing new or improved ways to address the weak areas. This paper serves to document the weak areas and methods developed to overcome or improve upon the weak areas. The improved methods will be incorporated into the 2005 version of the Aeroprediction Code and will be released later as the AP09. Several examples are given to show the improvement of the AP09 over the AP05 for configurations with and without boattails. The weapons affected (see Fig. 1) are primarily mortars, low-drag bombs, spin-stabilized projectiles, and some missiles.

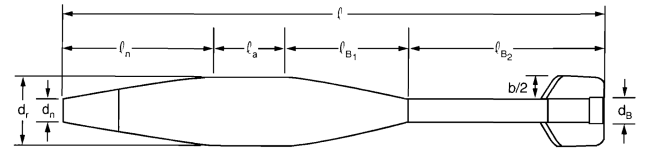

a) Typical mortar configuration

b) Schematic of Eight-Fin guided projectile

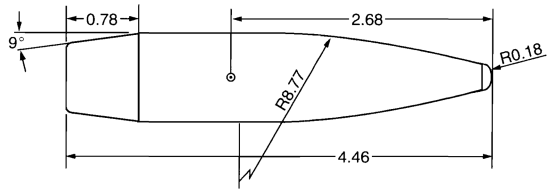

c) Spin-stabilized projectile (dimensions in calibers)

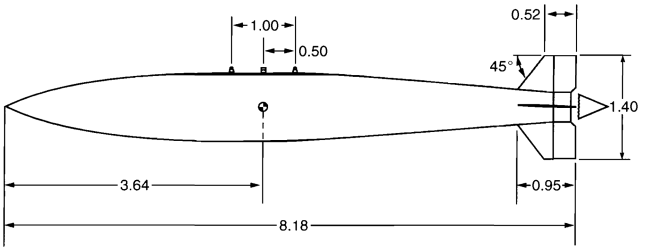

d) General purpose low-drag bomb (dimensions in calibers)

Fig. 1 Some typical weapons with boattails.

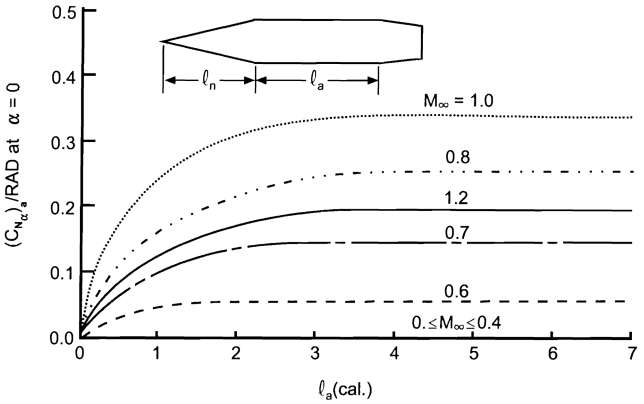

Fig. 2 Increase in (C_{N_α}) at subsonic and transonic Mach numbers due to afterbody.

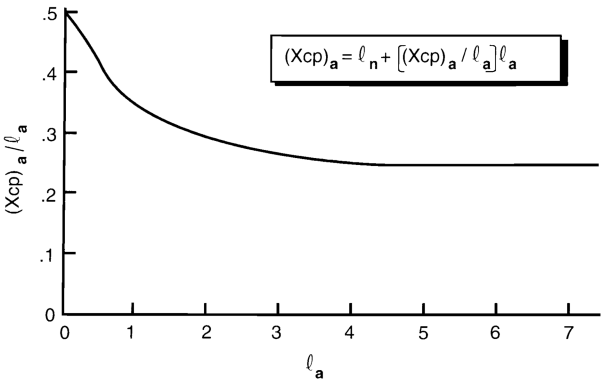

Fig. 3 Center of pressure of afterbody lift for $M_\infty < 1.2$.

New Improvements for AP09

This section of the paper will discuss improvements made to the AP05 that will be a part of the AP09. The weak areas will be dealt with individually in terms of modifications to existing methods or new technology developed and added to the AP09.

Body-Alone Lift Characteristics for $M_\infty < 1.2$

The body-alone normal-force characteristics of the Aeroprediction Code were all empirical. The center of pressure of the nose and boattail normal force were defined based on slender body theory (SBT) and the afterbody normal-force center of pressure was predicted empirically (see Chap. 4 of [2]). Each component of normal force and center of pressure will be reexamined. In investigating the nose component of normal force, the method of [2] was compared with the data of [3]. Rogers and Butler [3] provided data for short ogives as well as truncated ogives. It was found that even though the nose shape was anything but slender, the SBT value of 2.0 was actually more accurate than the method of [2], which was based primarily on experimental data for cones (see Fig. 4.21 of [2]). Hence, the method of [2] will be replaced by the SBT value of 2 for the nose component of normal-force coefficient slope near $\alpha = 0$. SBT will continue to be used for center of pressure prediction for the nose normal force at low-angle of attack (AOA). The additional normal force due to the presence of an afterbody and the normal-force center of pressure is predicted by the method of Wu and Aoyoma [4] transonically and empirically by the data of Spring [5] and Gwin and Spring [6] in the AP05 (again, see [2], p. 156). The only change in the AP09 will be to make the curve of Fig. 4.22, p. 156 of [2] for $M_\infty = 1.1$ and 1.2 for $M_\infty = 1.2$ only. The value for $M_\infty = 1.1$ is interpolated between the value at $M_\infty = 1.0$ and that for $M_\infty = 1.2$. The revised Fig. 4.22 of [2] and Fig. 4.24 of [2] are repeated here as Figs. 2 and 3, respectively.

The normal-force coefficient on the boattail was changed from the value used in the AP05 and prior versions of the Aeroprediction Code to that used in the AP09. Figure 4 gives the new values of the boattail normal-force coefficient slope for low-AOA and compares it with the older data [7,8]. The new curve of Fig. 4 is based on data from several more recent databases [9–12] than the databases used for the AP72 of Fig. 4. Note the new curve of Fig. 4 does not have quite as large of a negative value of C_{N_α} for the boattail as did the older curve. The AP05 used SBT for the center of pressure of the boattail. For most short boattails, SBT was adequate. However, for longer boattails, SBT values of center of pressure were found to be too far aft. As a result, a value closer to the intersection of the afterbody and boattail was chosen. This value is defined by Equation (1a).

$$(X_{\text{c.p.}}) = \ell - C\ell_B \tag{1a}$$

where $\ell_B \leq 1.0$ cal, $C = 0.75$

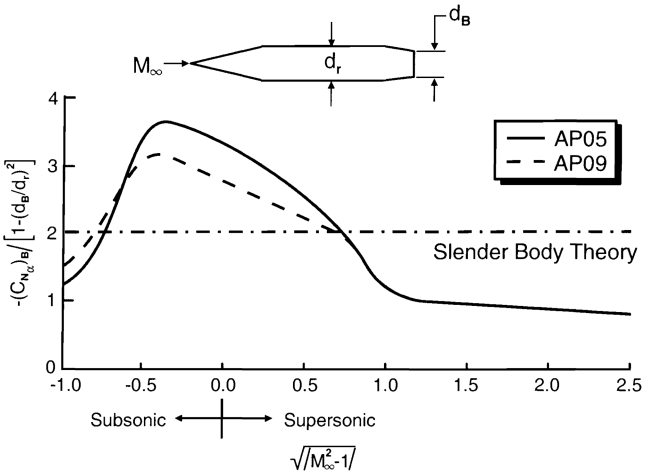

Fig. 4 Decrease in (C_{N_α}) due to boattail.

$$\left.\begin{array}{l} 1.0 < \ell_B \le 2.0 \\ 0.5 < M_\infty < 1.2 \end{array}\right\} C = (0.243 - 0.286M_\infty)\ell_B + 0.507 + 0.286M_\infty$$

$$\left.\begin{array}{l} 1.0 < \ell_B \le 2.0 \\ M_\infty \le 0.5 \end{array}\right\} C = 0.65 + .1\ell_B$$

$$\left.\begin{array}{l} \ell_B > 2.0 \\ 0.5 < M_\infty < 1.2 \end{array}\right\} C = 0.993 - 0.286M_\infty \qquad \left.\begin{array}{l} \ell_B > 2.0 \\ M_\infty \le 0.5 \end{array}\right\} C = 0.85$$

In addition to the Eq. (1a) center of pressure change for boattails, it was found that an upper bound on magnitude of boattail normal force computed from Fig. 4 was needed. This upper value was

$$\left.\begin{array}{l} \lfloor (C_{N_\alpha})_b \rfloor_{\max} = -1.5 + 0.2M_\infty, \\ \qquad 0.5 < M_\infty < 1.2 \\ = -1.5, M_\infty \le 0.5 \end{array}\right\} \tag{1b}$$

To summarize the new body-alone lift characteristics for Mach numbers less than 1.2, we have the following:

$$\left.\begin{array}{l} (C_{N_\alpha})_n = 2.0; (X_{\text{c.p.}})_n = \ell_n - \frac{(\text{vol})_n}{\pi R_r^2} \\ (C_{N_\alpha})_a = \text{Figure 2}; (X_{\text{c.p.}})_a = \text{Figure 3} \\ (C_{N_\alpha})_b = \text{Figure 4}; (X_{\text{c.p.}})_b = \text{Equation (1A)} \\ \qquad + \text{Equation (1B)} \end{array}\right\} \tag{1c}$$

The pitching moment coefficient derivative is then

$$C_{M_\alpha} = -\lfloor (C_{N_\alpha})_n (X_{\text{c.p.}})_n + (C_{N_\alpha})_a (X_{\text{c.p.}})_a + (C_{N_\alpha})_b (X_{\text{c.p.}})_b \rfloor \tag{2}$$

The total normal-force coefficient derivative and center of pressure for the body is then

$$C_{N_\alpha} = (C_{N_\alpha})_n + (C_{N_\alpha})_a + (C_{N_\alpha})_b \tag{3}$$

$$X_{\text{c.p.}} = -\frac{C_{M_\alpha}}{C_{N_\alpha}} \tag{4}$$

Body-Alone Lift Characteristics for $M_\infty \ge 1.2$

The best way to illustrate the problem that the hybrid theory of Van Dyke (HTVD) has in predicting the normal-force coefficient derivative at low-AOA correctly for a boattailed configuration is to compare the pressure coefficients to experimental data or a more accurate Navier–Stokes model. Figure 5 (taken from [2] as Fig. 3.6) compares the pressure coefficients predicted by the second-order Van Dyke (SOVD) method [13] on a sharp 10 deg cone cylinder at 0 deg AOA at a Mach number of 2.0. Note the excellent agreement of pressure prediction to experimental data. This excellent agreement of theory and experiment is the reason the SOVD method gives good axial-force prediction.

Figure 6 (taken from [2] as Fig. 3.7) shows the comparison of the HTVD (which combines a second-order accurate axial force predictor with a first-order accurate normal-force predictor) to experimental data on the same cone cylinder of Fig. 5, except the Mach number is 2.07 and AOA is 12 deg. Note the prediction of pressure by the hybrid theory is still quite good on the cone, but starts to deviate on the afterbody. Unfortunately, the authors were unable to find pressure coefficient data for a nose-cylinder-boattail configuration. However, suffice it to say, that if the afterbody pressure coefficients deviate from experimental data, as in Fig. 6, then the pressure prediction on the boattail will also deviate.

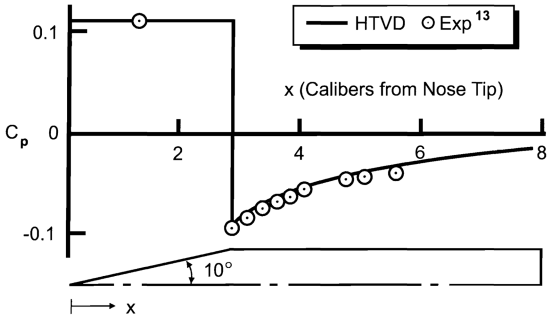

Fig. 5 Pressure coefficient on cone cylinder ($M_\infty = 2.00, \alpha = 0$ deg).

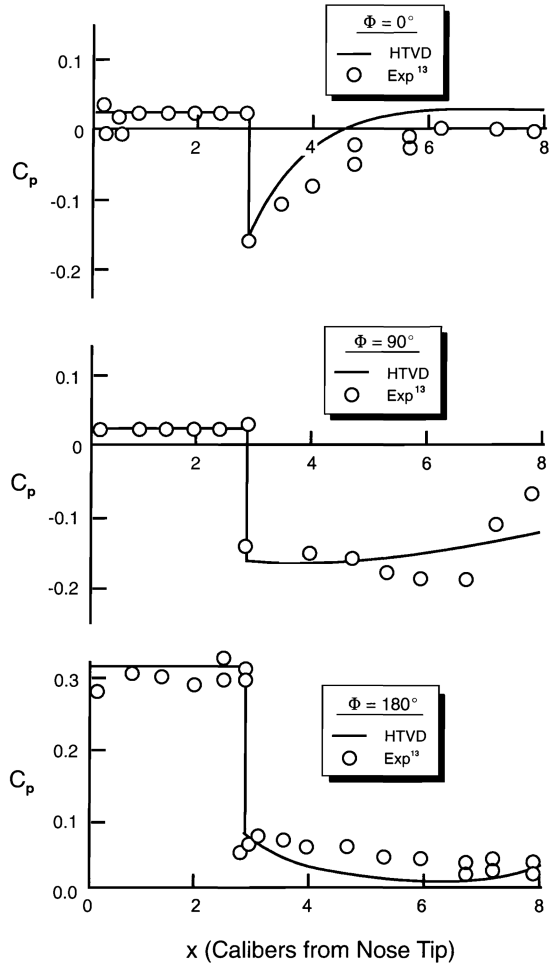

Fig. 6 Pressure coefficient on cone cylinder ($M_\infty = 2.07, \alpha = 12$ deg) of Fig. 5.

The Aeroprediction Code allows a nose-cylinder-boattail/flare for Mach numbers where the SOVD theory is used. The nose allows two sections. If subscripts 1, 2 denote the two nose sections, and subscripts 3 and 4 denote the cylinder and boattail/flare sections, respectively, then a method to correct the prediction of the forces and moments of the SOVD was found to be

$$C_{N_B} = C_{N_{\text{BN}}} + C_{N_1} + C_{N_2} + C_{N_3} + (\text{BF})C_{N_4} \tag{5a}$$

$$C_{M_B} = C_{M_{\text{BN}}} + C_{M_1} + C_{M_2} + C_{M_3} + (\text{BF})C_{M_4} \tag{5b}$$

The first term of Eq. (5) is the normal force and pitching moment on the blunt nose if the configuration has a blunt nose. The next two terms of Eq. (5) are the normal force and pitching moment of the two nose segments, the fourth term is the afterbody normal force and pitching moment, and the last term is the normal force and pitching moment of the boattail or flare. The boattail factor (BF) was defined by trial and error on configurations [9–12] that have boattails as

$$\left.\begin{array}{l} \text{BF} = \left(1 - \frac{M_\infty}{2}\right)\frac{\ell_B}{2} + \frac{3M_\infty}{4} - \frac{1}{2}; 1.0 \le \ell_B \le 3.0 \\ \text{BF} = \frac{M_\infty}{2}; \ell_B < 1.0 \\ \text{BF} = 1.0; M_\infty \ge 2.0 \\ \text{BF} = 1.0; \ell_B > 3.0 \\ \text{BF} = 1.0; r_B \ge r_r \end{array}\right\} \tag{5c}$$

In examining Eq. (5c), it is seen that the boattail factor is one (i.e., no change from the AP05) if either Mach number is greater than 2.0, boattail length ℓ_B is greater than 3.0 cal, or the configuration has a flare ($r_B \geq r_r$) vs a boattail. One may naturally ask, if the pressure prediction of the boattail leads to consistent errors in normal force and pitching moment, will there not be errors in axial force coefficient prediction as well? The answer is yes, but the normal force and pitching moment coefficient errors are larger and easier to isolate, whereas the axial force errors are small enough that good axial force prediction accuracy is still obtained on boattailed configurations. Hence, no attempt was made to develop a correction for axial force coefficient predictions of the SOVD theory.

Body-Alone Pitch Damping Characteristics for Configurations with Long Boattails

The body-alone pitch damping is empirical and based on the SPINNER code of the early 70s [7]. The body-alone pitch damping was improved upon [14] for the AP02. The improvements were aimed at longer bodies, higher Mach numbers, and configurations with flares. However, when a body has a long boattail, the pitch damping is decreased drastically and the improved methodology of [14] does not account for the long boattail. When a configuration has a long boattail, the pitch damping is decreased for two reasons. First, the body pitch damping is based on body planform area, which is decreased when a boattail is present. Second, the rotational portion of the pitch damping is decreased even more due to the fact that the pitch damping is proportional to the normal-force component of a segment of the body times the distance of that segment from the center of moments squared. The boattail area decreases as the distance from the center of moments increases. The combination of the aforementioned two phenomenons means the body-alone pitch damping methodology of the AP05 needs to be modified for configurations with long boattails.

The method chosen to address the AP05 weakness on body-alone pitch damping prediction for long boattails was to define a factor to multiply the AP05 prediction that was a function of base diameter, center of moment location, and Mach number. It was found in comparing the AP05 C_{M_q} predictions to data that these were the most important variables. Thus,

$$(C_{M_q})_{09} = (C_{M_q})_{05}\left(\frac{r_B}{r_r}\right)^x \tag{6}$$

where $(C_{M_q})_{09}$ and $(C_{M_q})_{05}$ represent the AP09 and AP05 predictions for pitch damping, respectively. The factor $(r_B/r_r)^x$ of Eq. (6) was derived based on comparisons to data.

We also know that when $(r_B/r_r) > 0.85$, we have good agreement of AP05 pitch damping to data. Hence, the exponent x of Eq. (6) should go to zero when r_B/r_r increased above about 0.85. We also know that as the center of moment moves toward the nose, the AP05 C_{M_q} predictions get worse because the loss of planform area from the long boattail gets farther from the center of moments. Thus, the exponent x of Eq. (6) will get larger as the center of moments moves forward.

Table 1 gives the final methodology derived for the exponent x of Eq. (6). Note that in Table 1, three cases are considered for center of mass location:

$$\frac{X_{\text{c.g.}}}{L} \leq 0.44 \qquad \frac{X_{\text{c.g.}}}{L} \geq 0.55 \qquad 0.44 < \frac{X_{\text{c.g.}}}{L} < 0.55$$

A forward location of $X_{\text{c.g.}}/\ell$ of 0.44 and an aft location of $X_{\text{c.g.}}/\ell$ of 0.55 are fairly practical values of center of gravity extremes for weapons. Most configurations with long boattails fall in the $X_{\text{c.g.}}/\ell \leq 0.44$ category and configurations with short boattails typically fall in the $X_{\text{c.g.}}/\ell \geq 0.55$ category. As seen in Table 1, the exponent x of Eq. (7) tends to zero as r_B/r_r approaches one and also gets larger with more forward values of $X_{\text{c.g.}}/\ell$. Of course, the AP05 code already has an upper limit of boattail angle of 8 deg which is used in implementation of Eq. (6).

Multifin Factors for Low Aspect Ratio Wings at Subsonic Speeds

The new multifin factors for configurations with six and eight fins are given in Table 2. The only change in these factors from the AP05 [1] is for the $M_\infty \leq 0.6$ column for the aspect ratio of 2.0 and less. Note the new values are now more in line with the Navier–Stokes computations of Table 2 for $M \geq 1.5$, as opposed to much higher values previously used in the AP05 which were based on unsteady Euler computations. The reader is referred to [2], pp. 429–447 for a

Table 1 Methodology for body-alone pitch damping for configurations with long boattails

1.	$X_{\text{c.g.}}/l \leq 0.44$
	$M_\infty \leq 1.0$
	$X_2 = 2.3$
	IF $(r_B/r_r) > 0.5, X_2 = 4.16 - 3.71(r_B/r_r)$
	IF $(r_B/r_r) > 0.85, X_2 = 1.0$
	$M_\infty \geq 2.0$
	$X_2 = 1.8$
	IF $(r_B/r_r) > 0.5, X_2 = 2.94 - 2.29(r_B/r_r)$
	IF $(r_B/r_r) > 0.85, X_2 = 1.0$
	$1.0 < M_\infty < 2.0$
	$X_2 = 2.8 - 0.5M_\infty$
	IF $(r_B/r_r) > 0.5, X_2 = [4.16 - 3.71(r_B/r_r)](2.0 - M_\infty) + [2.94 - 2.29(r_B/r_r)](M_\infty - 1)$
	IF $(r_B/r_r) > 0.85, X_2 = 1.0$
2.	$X_{\text{c.g.}}/l \geq 0.55$
	$X_2 = 1.7$
	IF $(r_B/r_r) > 0.5, X_2 = 2.7 - 2.0(r_B/r_r)$
	IF $(r_B/r_r) > 0.85, X_2 = 1.0$
3.	$0.44 < X_{\text{c.g.}}/l < 0.55$
	Linear interpolate between methodology for $X_{\text{c.g.}}/L \leq 0.44$ and $X_{\text{c.g.}}/L \geq 0.55$ based on value of $X_{\text{c.g.}}/L$
4.	Blend large boattail to small boattail
	IF $(r_B/r_r) \leq 0.65, P_3 = 1.0$
	IF $(r_B/r_r) > 0.65, P_3 = -50.2 + 173.0(r_B/r_r) - 189.6(r_B/r_r)^2 + 68.8(r_B/r_r)^3$
	IF $P_3 > 2.0, P_3 = 2.0$
	$X_3 = 2.0 - P_3$
5.	Final equation
	$x = (X_2)(X_3)$
	$(C_{M_q})_{09} = (C_{M_q})_{05}(r_B/r_r)^X$

Table 2 Approximated values of the factors F_6 and F_8 obtained from smoothed values of the ZEUS and GASP code computations and engineering judgement

AR	α	Mach number for F_6					Mach number for F_8				
		0.6	1.5	2.0	3.0	4.5	0.6	1.5	2.0	3.0	4.5
	0.0	1.26	1.37	1.27	1.19	1.22	1.42	1.42	1.40	1.27	1.20
	15	1.00	1.00	1.10	1.19	1.35	1.21	1.03	1.17	1.27	1.35
	30	1.00	1.00	1.00	1.19	1.22	1.00	1.00	1.01	1.27	1.22
	45	1.00	1.00	1.00	1.00	1.00	1.00	1.00	1.00	1.00	1.00
	60	1.00	1.00	1.00	1.00	1.00	1.00	1.00	1.00	1.00	1.00
	75	1.00	1.00	1.00	1.00	1.00	1.00	1.00	1.00	1.00	1.00
0.25	90	1.00	1.00	1.00	1.00	1.00	1.00	1.00	1.00	1.00	1.00
	0.0	1.26	1.25	1.20	1.30	1.47	1.44	1.36	1.28	1.35	1.72
	15	1.05	1.10	1.15	1.29	1.50	1.22	1.18	1.24	1.40	1.83
	30	1.00	1.00	1.07	1.29	1.36	1.00	1.08	1.16	1.41	1.60
	45	1.00	1.00	1.00	1.00	1.00	1.00	1.00	1.04	1.06	1.20
	60	1.00	1.00	1.00	1.00	1.00	1.00	1.00	1.00	1.00	1.00
	75	1.00	1.00	1.00	1.00	1.00	1.00	1.00	1.00	1.00	1.00
0.50	90	1.00	1.00	1.00	1.00	1.00	1.00	1.00	1.00	1.00	1.00
	0.0	1.28	1.22	1.35	1.42	1.50	1.50	1.38	1.58	1.96	2.00
	15	1.15	1.13	1.23	1.32	1.50	1.34	1.38	1.38	1.80	2.00
	30	1.06	1.00	1.00	1.21	1.38	1.10	1.28	1.15	1.64	2.00
	45	1.02	1.00	1.00	1.10	1.13	1.00	1.05	1.00	1.48	1.61
	60	1.00	1.00	1.00	1.00	1.00	1.00	1.00	1.00	1.32	1.25
	75	1.00	1.00	1.00	1.00	1.00	1.00	1.00	1.00	1.16	1.00
1.0	90	1.00	1.00	1.00	1.00	1.00	1.00	1.00	1.00	1.00	1.00
	0.0	1.42	1.50	1.50	1.50	1.50	1.68	1.77	1.97	1.92	1.90
	15	1.31	1.41	1.27	1.39	1.50	1.52	1.95	1.75	1.77	2.00
	30	1.17	1.00	1.03	1.27	1.45	1.35	1.65	1.57	1.62	2.10
	45	1.03	1.00	1.00	1.14	1.23	1.18	1.32	1.27	1.47	1.95
	60	1.00	1.00	1.00	1.00	1.00	1.02	1.00	1.02	1.32	1.62
	75	1.00	1.00	1.00	1.00	1.00	1.00	1.00	1.00	1.17	1.32
2.0	90	1.00	1.00	1.00	1.00	1.00	1.00	1.00	1.00	1.00	1.00
	0.0	1.50	1.50	1.50	1.50	1.50	2.00	1.90	2.00	2.00	2.00
	15	1.33	1.41	1.27	1.39	1.50	1.70	1.95	1.75	1.77	2.00
	30	1.17	1.00	1.03	1.27	1.45	1.47	1.65	1.57	1.62	2.00
	45	1.03	1.00	1.00	1.14	1.23	1.25	1.32	1.27	1.47	1.95
	60	1.00	1.00	1.00	1.00	1.00	1.02	1.00	1.02	1.32	1.62
	75	1.00	1.00	1.00	1.00	1.00	1.00	1.00	1.00	1.17	1.32
4.0	90	1.00	1.00	1.00	1.00	1.00	1.00	1.00	1.00	1.00	1.00

full discussion of the derivation, computation, and use of the multifin factors for configurations with six or eight fins. Moore and Hymer [1] then modified some of those factors slightly. Table 2 represents a revision of the results in [1,2].

It is speculated that the reason the inviscid values for aspect ratio 4, which have been previously validated, are much higher than the multifin factors for the lower aspect ratio is viscous effects. The Navier–Stokes code automatically includes boundary-layer displacement effect, which is much more important on fins that have a small span than on fins with a larger span. Thus, the low aspect ratio values of the multifin factors, which had not been previously validated for $M_\infty < 1.0$, were modified in accordance with data and are now more in line with the supersonic multifin factors computed from a full Navier–Stokes code.

Linear Roll and Pitch Damping Improvements for Finned Configurations with Long Boattails

Both pitch and roll damping of fins at zero AOA are computed by linearized theory and assumes the fins go all the way to the body centerline. This approach of computing pitch and roll damping of fins when the fins are on a cylindrical body works well. However, when the fins lie on a long boattail, the fin span needs to be reduced to an effective span to account for the low dynamic pressure and viscous effects in the vicinity of the body. Including boundary-layer displacement thickness (BLDT) effects had little effect on either the roll or pitch damping because any reduction in fin span was compensated for by the equivalent increase in body radius. That is, if the span of the wings for roll and pitch damping computations is

$$b_1 = b + 2r_B \tag{7}$$

and we decrease b by twice the BLDT and increase r_B by the BLDT, the net result is no change in dynamic derivatives.

The approach used in the AP09 is therefore to define effective values of the radius where the tail on the boattail is located. For pitch damping calculations, this effective radius is

$$(R_B)_{\text{eff}} = [1 + C_1(M)]\, r_W - C_1(M) r_r \tag{8a}$$

where

$$C_1(M) = 0.33; \qquad M_\infty \le 0.6 = 0.33 - 0.55(M_\infty - 0.6)$$
$$0.6 < M < 1.2 = 0; \qquad M_\infty \ge 1.2$$

In examining Eq. (8), it is seen that for $M_\infty > 1.2$, the effective radius becomes r_W, the body radius at the wing midchord, which is the current value of r in the AP05.

For roll damping, the effective radius is

$$(r_B)_{\text{eff}} = 1.20 r_B - 0.20 r_r \tag{8b}$$

Equation (7) now becomes

$$b_1 = b + 2(r_B)_{\text{eff}} \tag{9}$$

and Eq. (8a) and (8b) define $(r_B)_{\text{eff}}$ for pitch and roll damping calculations, respectively, at all Mach numbers. Both Eqs. (8a) and (8b) were derived based on numerical experiments applying the AP05 code and comparing the resulting computations to experiment.

It was mentioned earlier that the body length under the wing was used in computing roll damping and pitch damping, even though, for the dynamic derivatives, the wing was assumed to go all the way to

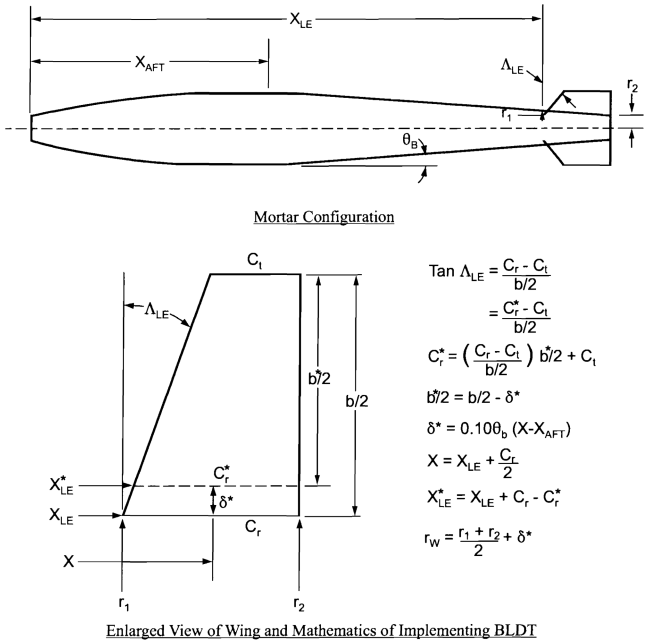

Fig. 7 Geometry involved in incorporating boundary-layer displacement thickness effects into wing lift calculations.

the body centerline. To avoid the double counting of body length and area for dynamic derivatives, the root chord length was subtracted from the overall body length. That is

$$\ell_1 = \ell - c_{r_W} \tag{10}$$

Equation (10) will affect dynamic derivatives of all configurations with lifting surfaces present.

Table 3 Values of the axial force AOA parameters for a body–tail configuration

M_∞	$f'(M,0)$	$F(M,30)$	$F(M,60)$	$F(M,90)$
0.0	0.20	−0.16	−0.79	−0.060
0.6	0.20	−0.16	−0.66	−0.060
0.8	0.15	−0.160	−0.46	−0.060
0.9	0.12	−0.135	−0.38	−0.060
1.0	0.120	−0.110	−0.26	−0.060
1.15	0.160	−0.020	−0.18	−0.140
1.2	0.186	0.0	−0.12	−0.160
1.3	0.200	0.040	−0.06	−0.220
1.5	0.258	0.100	0.06	−0.240
2.0	0.330	0.150	0.20	−1.130
2.5	0.350	0.180	0.28	−0.060
3.0	0.346	0.190	0.30	0.0
3.5	0.352	0.200	0.32	0.30
4.5	0.230	0.220	0.33	0.065
≥ 6.0	0.180	0.230	0.34	0.070

Incorporation of Boundary-Layer Displacement Effects on Body-Tail Configurations with Long Boattails

The AP05 and prior versions of the Aeroprediction Code have a boundary-layer displacement model included for boattails. This model has two elements. The first element reduces the boattail to a maximum of 8 deg if the boattail angle is greater than 8 deg. The second part of the model reduces the boattail angle by 10%. That is

$$(\theta_b)_{\text{eff}} = 0.9\theta_b \tag{11}$$

where θ_b is the actual boattail angle and $(\theta_b)_{\text{eff}}$ is the reduced angle due to BLDT. In applying the model represented by Eq. (11) to configurations with long boattails, it was found that only one additional criterion was needed. The additional criterion was to put an upper bound on the maximum allowable negative value of normal-force coefficient derivative for the boattail for $M_\infty < 1.0$. The maximum value for $(C_{N_\alpha})_b$ is approximated by

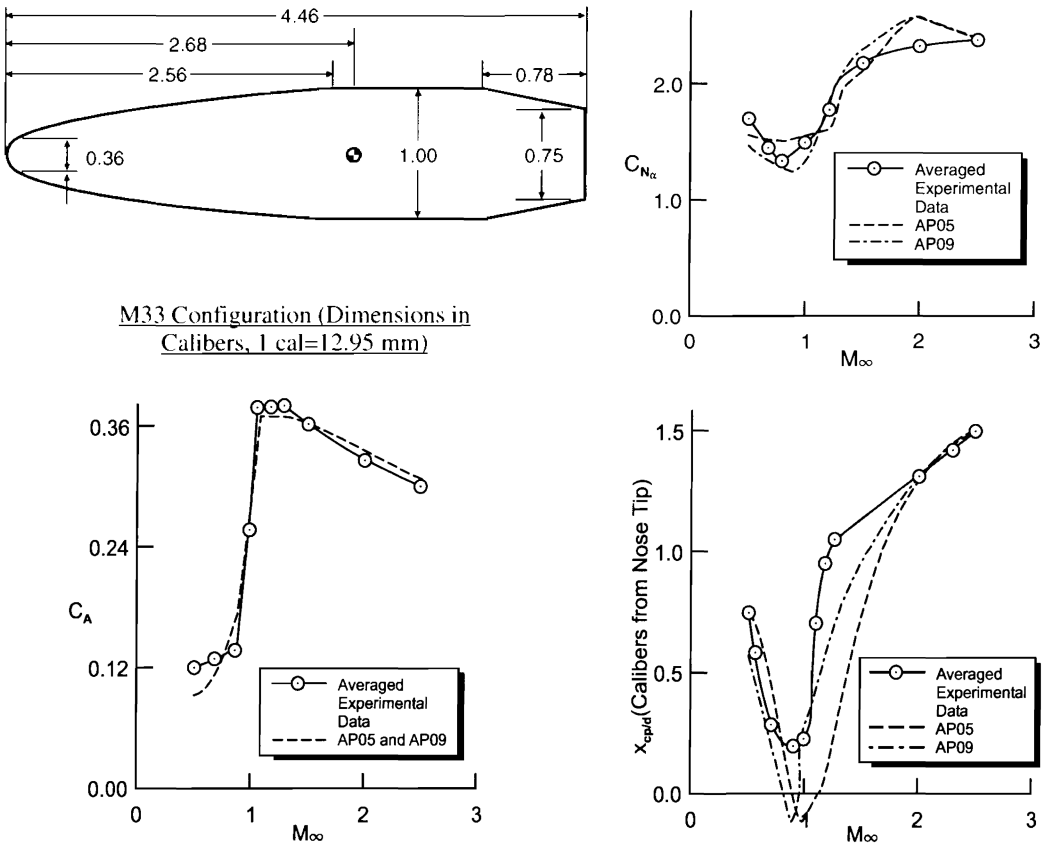

Fig. 8 Comparison of AP05 and AP09 aerodynamic predictions to experimental data [10] for M33 projectile.

Table 4 Error comparisons of AP05 and AP09 aerodynamics to data [10] for the M33 projectile

M_∞	C_A errors, %		$(C_{N_\alpha})_{\alpha\approx 0}$ errors, %		$X_{\text{c.p.}}/d$ errors, % of body length	
	AP05	AP09	AP05	AP09	AP05	AP09
0.5	19.2	19.2	6.7	9.6	0.2	4.3
0.6	17.9	17.9	1.9	8.4	0.7	5.8
0.7	11.7	11.7	5.5	5.5	3.4	5.4
0.8	1.5	1.5	10.4	0.7	2.2	4.9
0.9	15.0	15.0	15.7	1.4	3.1	6.3
1.0	16.4	16.4	4.0	3.3	7.2	1.8
1.1	2.7	2.7	1.2	4.3	15.2	6.5
1.2	2.1	2.1	8.5	4.5	19.3	8.3
1.3	0.5	0.5	4.7	5.2	16.4	7.6
1.4	1.0	1.0	3.9	5.4	13.7	6.5
1.5	2.2	2.2	3.2	5.0	11.4	5.4
1.6	2.0	2.0	0.9	6.3	8.1	4.0
1.7	1.4	1.4	4.0	7.8	5.4	2.7
1.8	0.9	0.9	6.6	8.7	2.9	1.6
1.9	0.3	1.3	8.6	9.5	0.7	0.2
2.0	1.2	1.2	9.8	9.8	0.9	0.9
2.1	1.6	1.6	8.1	8.1	0.7	0.7
2.2	1.6	1.6	5.9	5.9	0.2	0.2
2.3	2.3	2.3	3.8	3.8	0.2	0.2
2.4	2.6	2.6	1.3	1.3	0.5	0.5
2.5	3.0	3.0	0	0	0.7	0.7
Avg	5.1	5.1	5.5	5.5	5.4	3.5

$$(C_{N_\alpha})_b = -1.5 + 0.2M_\infty \tag{12}$$

for $M_\infty < 1.2$. For $M_\infty \geq 1.2$, the hybrid theory of Van Dyke computes the value of $(C_{N_\alpha})_b$ for Mach numbers up to about 2.0 and the second-order shock expansion theory calculates $(C_{N_\alpha})_b$ for Mach numbers of about 2.0 and higher. All theoretical methods and empirical methods use Eq. (11) with the upper values of θ_b reduced to 8 deg before Eq. (11) is applied. In other words, the body boattail shape is changed before pressure coefficients are computed. The Eq. (11) approach for accounting for BLDT has been shown to give reasonable results over a wide range of boattail shapes.

The main problem with the AP05 and all prior versions of the Aeroprediction Code is that the BLDT is not accounted for in wing span reduction. It was discussed how the fin span reduction effects were included in the roll and pitch damping computations. However, for lift computations, the wing span does not include the body radius

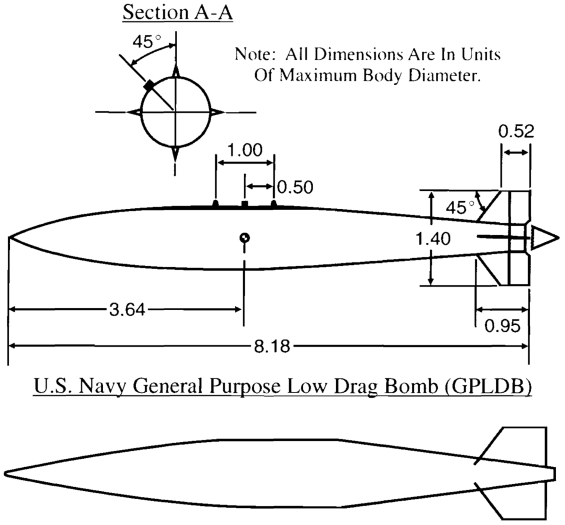

Fig. 9 U.S. Navy low-drag bomb and AP09 representation.

Table 5 Comparison of average static aerodynamic prediction errors of AP05 and AP09 compared with experimental data for four boattailed projectiles

Configuration	C_A errors, %		AP09 imp. over AP05, %	C_{N_α} errors, %		AP09 imp. over AP05, %	$X_{\text{c.p.}}/d$ errors, % of body length		AP09 imp. over AP05, %
	AP05	AP09		AP05	AP09		AP05	AP09	
1) 155 mm [9]	6.9	6.9	0.0	4.6	3.4	26.4	6.1	5.2	14.8
2) M33 [10]	5.1	5.1	0.0	5.5	5.5	0.0	5.4	3.5	35.2
3) 5"/54 MK41 [11]	7.9	7.9	0.0	7.2	4.2	41.7	9.8	6.5	33.7
4) Hi Frag [12]	5.0	5.0	0.0	12.6	3.9	67.4	8.2	1.2	85.4
Average	6.2	6.2	0.0	7.5	4.3	42.7	7.4	4.1	44.6

Table 6 Comparison of average static and dynamic aerodynamic prediction errors of AP05 and AP09 compared with experiment for several mortar rounds

Mortar static aerodynamics summary									
Configuration	C_A errors, %		AP09 imp. over AP05, %	C_N errors, %		AP09 imp. over AP05, %	$X_{\text{c.p.}}/d$ errors, % of body length		AP09 imp. over AP05, %
	AP05	AP09		AP05	AP09		AP05	AP09	
1) 81 mm [26]	10.1	9.5	5.9	33.3	13.7	58.9	2.6	1.4	46.0
2) XM 984 (194441)[15]	15.1	11.8	21.9	24.5	13.2	46.1	5.3	6.3	−18.2
3) XM 984 (194541) [15]	14.4	11.5	20.1	12.4	5.1	58.9	6.8	5.8	14.7
4) PGMM (11111) [16]	12.2	17.5	−43.4	27.8	14.1	49.3	7.6	2.1	72.3
5) PGMM (51511) [17]	13.1	19.6	−49.6	30.1	14.7	51.2	6.8	2.4	64.7
6) M49A4 [18]	21.6	12.7	41.2	35.6	11.1	68.8	77.0	6.7	91.3
Average	14.4	13.8	4.2	27.3	12.0	56.0	17.7	4.1	76.8

Mortar dynamic aerodynamics summary						
Configuration	C_{ℓ_p} errors, %		AP09 improvement over AP05, %	C_{M_q} errors, %		AP09 improvement over AP05, %
	AP05	AP09		AP05	AP09	
1) 81 mm mortar [19]	40.1	13.0	67.6	232.4	7.4	96.8
2) PGMM (11111) [16]	104.5	35.5	66.0	288.3	13.3	95.3
3) PGMM (51511) [17]	102.3	33.7	61.1	204.8	8.5	95.8
Average	82.3	27.4	66.7	241.8	9.7	96.0

and, instead, wing–body and body–wing interference effects are included to get the complete lift computations. To include the BLDT in wing lift calculations, we need to decrease the wing semispan by the BLDT, decrease the wing root chord slightly, increase the distance from the nose to the wing leading edge slightly, and increase the radius at the wing by the BLDT. Figure 7 illustrates physically what is changed for the wing–body geometry when BLDT is included. In Fig. 7, X is the distance to the midpoint of the root chord (or centroid of wing area if available) from the nose tip and X_{AFT} is the distance from the nose tip to the start of the boattail.

The geometry of Fig. 7 is "hardwired" into the AP09. Thus, the code user will simply put in the configuration geometry as in the AP05. However, the AP09 has logic based on whether the configuration has a boattail or not. If the configuration has a boattail with a fin on it, the geometry of Fig. 7 is automatically used for wing lift calculations. The effect of including BLDT into the aerodynamic calculations is to reduce wing normal force, axial force, pitching moment, and configuration static stability. The amount of the decrease is dependent on the boattail angle and length.

Nonlinear Axial Force Modifications for Body-Tail Configurations

The nonlinear axial force coefficient at AOA was summarized in [2] (pp. 258–265). The approach used in the AP05 for the nonlinear axial force term is to define the term empirically based on databases. That is

$$C_A = C_{A_0} + f(M_\infty, \alpha) \tag{13}$$

where C_{A_0} is the value calculated for axial force at zero AOA and $f(M_\infty, \alpha)$ is the nonlinear term given by

$$f(M_\infty \alpha) = A\alpha + B\alpha^2 + C\alpha^3 + D\alpha^4 \tag{14}$$

The constants A, B, C, and D are defined based on the conditions $f'(M_\infty, 0)$, $f(M_\infty, 30)$, $f(M_\infty, 60)$, and $f(M_\infty, 90)$. The values of the parameters $f'(M_\infty, 0)$ and $f(M_\infty, 30)$ are modified slightly for the body–tail case at low Mach numbers using [15–25] and are now closer to the values for the body-alone configuration. No changes were made to the body-alone and wing–body–tail case. The new values of $f(M_\infty, \alpha)$ for body–tail cases are given in Table 3.

Results and Discussion

Many of the configurations that aerodynamics were available for are limited distribution. The limited distribution statement is generally for Department of Defense (DOD) agencies and the DOD contractors. As a result, for configurations that have limited distribution statements or have proprietary information, no aerodynamics or configuration geometry will be shown. The references for each case will be given for those who want to view the configurations and their aerodynamics and are able to access the reports. For limited distribution configurations, error comparisons can be given for each configuration. Results of the AP05 and AP09 aerodynamic predictions compared with experimental data will be shown in terms of the error comparisons. Here, the errors are defined for each aerodynamic coefficient as

$$\text{percent error} = \frac{|C_{\mathrm{exp}} - C_{\mathrm{theory}}|}{C_{\mathrm{exp}}} \times 100 \tag{15}$$

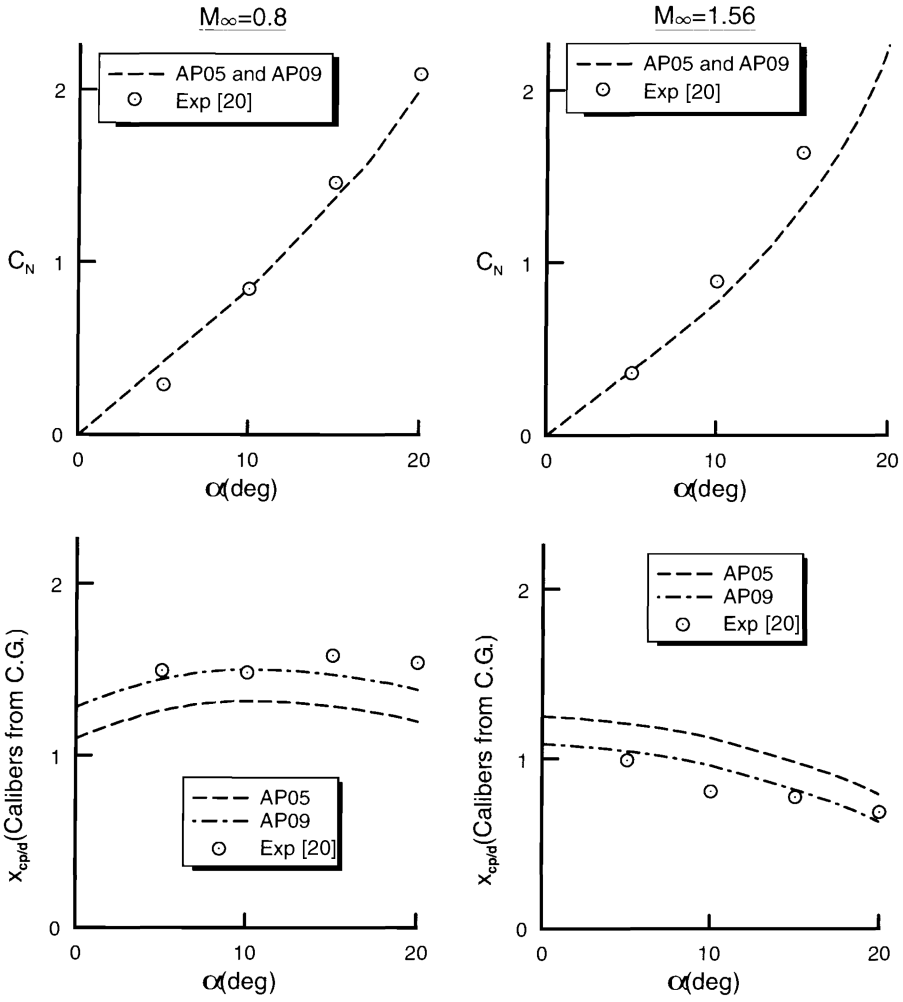

Fig. 10 Normal force and center of pressure comparisons of AP05 and AP09 to experiment ($\Phi = 0$ deg).

For center of pressure, the errors will be defined in terms of percent of body length. That is,

$$\frac{[(X_{\text{c.p.}})/d]_{\text{error}}}{\ell} = \frac{|[(X_{\text{c.p.}})_{\text{exp}}/d] - [(X_{\text{c.p.}})_{\text{theory}}/d]|}{\ell} \times 100 \qquad (16)$$

The errors of Eq. (15) and (16) can be defined for C_A, $(C_{N_\alpha})_{\alpha\approx 0}$, and $X_{\text{c.p.}}/d$ for spin-stabilized projectiles and other weapons designed to fly at small AOA and then averaged for several Mach numbers. For weapons designed to fly at higher AOA, errors averaged over AOA and Mach numbers are more appropriate than averaging over Mach numbers only for low-AOA data.

In addition to error comparisons of the AP05 and AP09 compared with experimental data, improvements in error of the AP09 over the AP05 for various aerodynamic coefficients can be defined as

$$\text{AP09 improvement in aerodynamics over the AP05} = \frac{|\text{AP05 avg error}(\%) - \text{AP09 avg error}(\%)|}{\text{AP09 avg error}(\%)} \qquad (17)$$

Equation (17) can be used for each of the aerodynamic coefficients that were computed by each code.

Spin-Stabilized Projectiles

Four projectiles will be considered, the Army 155 mm [9], M33 [10], and the Navy 5"/54 [11] and Hi Frag [12] projectiles. Of the four projectiles, only the M33 is published in an unlimited distribution format. For the M33 configuration, aerodynamics and configuration geometry can be shown. All four projectiles have boattails, and so results with the AP05 and AP09 will differ, particularly for Mach numbers below 2.0.

The first configuration considered is the M33 projectile [10]. Figure 8 shows the M33 configuration along with comparisons of AP05 and AP09 predictions compared with experimental data. Because the data are averaged range data, values of C_{N_α} and $X_{\text{c.p.}}/d$ were computed at 2 deg AOA. Table 4 then gives the error comparisons of the AP05 and AP09 at each 0.1 Mach number interval for $M_\infty = 0.5$ to 2.5. The M33 configuration has a 0.78 cal boattail. Note in comparing the AP05 and AP09 predictions to averaged experimental data in Fig. 8, and more specifically in Table 4, that both the AP05 and AP09 give good predictions of C_A and C_{N_α}. However, the AP09 reduces the average center of pressure error of the AP05 from 5.4 to 3.5% of the body length. This 35% reduction in center of pressure error for the AP09 brings the overall average below the desired criteria of ±4% of body length.

Table 5 now averages the errors for four projectile configurations for both the AP05 and AP09 compared with data. As seen in the table, the overall axial force coefficient error for both the AP05 and AP09 is 6.2%. The normal-force coefficient slope error of the AP09 is 4.3% compared with 7.5% for the AP05, or a 42.7% reduction. The largest error reduction was for the Hi Frag projectile, which had the largest boattail. The average center of pressure error for the AP09 was 4.1%, close to the goal of ±4%, whereas the AP05 center of pressure error was 7.4%, well above the ±4% goal. The AP09 thus decreased the average center of pressure error of the AP05 by 44.6%.

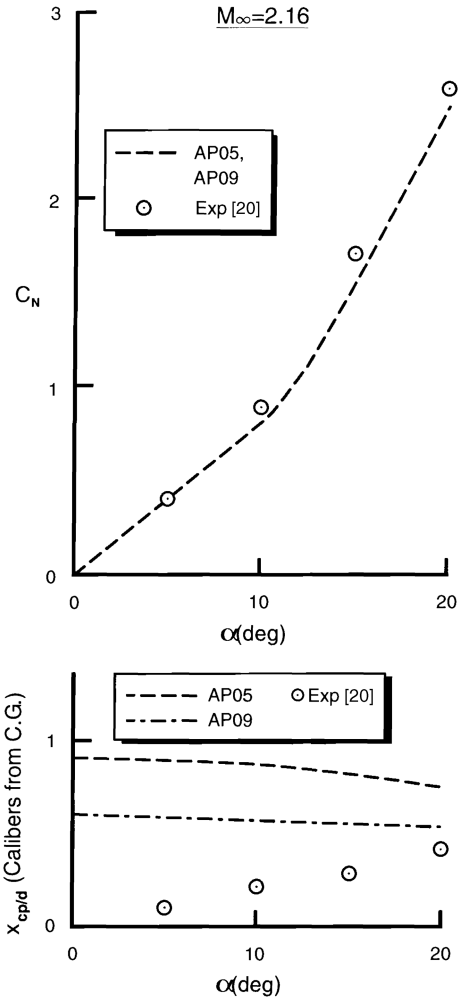

Fig. 11 Normal force and center of pressure comparisons of AP05 and AP09 to experiment for GPLDB ($\Phi = 0$ deg).

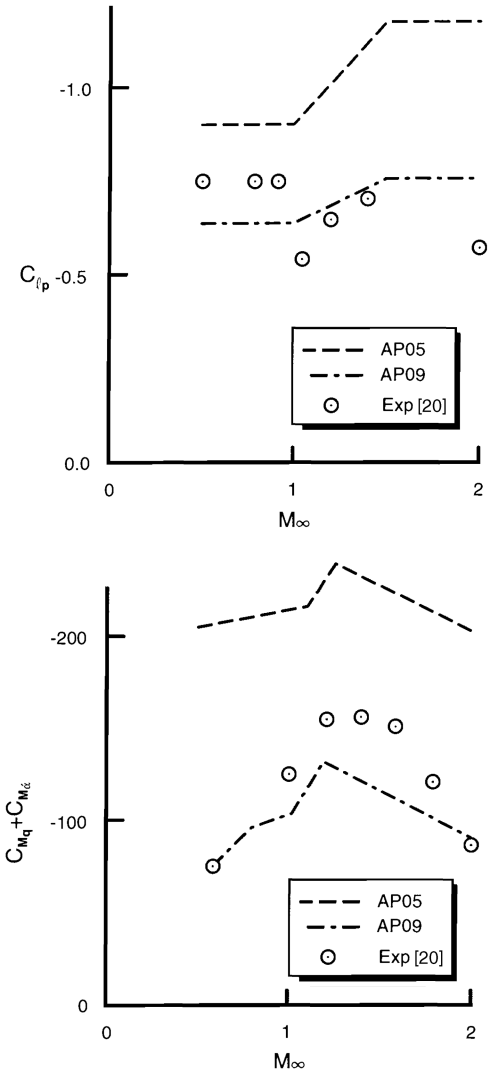

Fig. 12 Roll and pitch damping comparisons of AP05 and AP09 to experiment for GPLDB ($\Phi = 0$ deg).

In summary, the improvements in body-alone normal force and center of pressure prediction for projectile configurations with boattails has provided substantial improvement in the AP09 prediction accuracy for these coefficients compared with the AP05. The largest error improvements occurred for the longest boattail case. No changes in axial force prediction errors were seen between the AP05 and AP09 for spin-stabilized projectiles.

Mortar Configurations

Several mortar configurations will be considered to compare the AP09 static and dynamic aerodynamics to both the AP05 and experimental data. All mortar cases have a limited distribution statement, and so only errors of AP05 and AP09 predictions will be given. The specific configurations and their aerodynamics can be found in the references that are given for each case.

Most mortar configurations, as seen in Fig. 1, consist of a forebody, short afterbody, and boattail, followed by a boom with fins attached. The geometry of the mortar is only allowed exactly in the Aeroprediction Code where second-order-shock expansion theory is used, or around $M_\infty \leq 1.1$. On the other hand, typical mortar flight regimes are $M_\infty \leq 1.1$. The bottom line is that the mortar configuration must be forced into a nose, afterbody, boattail shape to allow the Aeroprediction Code to compute aerodynamics for $M_\infty \leq 2.0$. This means the boattail must be modified to include the length of the boom.

The user of the Aeroprediction Code can expect slightly higher errors for configurations in which the geometry is modified to fit within the context of the required nose, afterbody, boattail format than those configurations in which no geometry modifications are needed. It is the goal of the present paper to reduce the errors of the computation process as much as possible through the new methodology. The new methodology attempts to account primarily for the viscous effects present on mortars and other long boattail cases that the AP05 and prior versions of the Aeroprediction Code do not completely account for.

Table 6 gives a summary of the static and dynamic aerodynamic prediction errors of the AP05 and AP09 for mortar configurations. Note there are six configurations for static aerodynamics and only three for dynamic derivatives. As seen in the summary table, axial force coefficients for the AP09 are only slightly superior to the AP05, with the AP09 being superior on four cases and inferior to the AP05 on the other two configurations. The AP09 normal-force and center of pressure prediction, on average, are much better than the AP05. The AP05 normal-force prediction error is cut in half by the AP09 (12.0 vs 27.3%) and the center of pressure error is reduced by over 75% (4.1 vs 17.7% of body length). The area of largest improvement of the AP09 over the AP05 is dynamic derivatives. The C_{ℓ_p} errors are reduced from 82.3 to 27.4% and the C_{M_q} errors are reduced from 241.8 to 9.7% when using the AP09 compared with the AP05. It is therefore clear that the AP09 shows substantial improvement over the AP05 on all mortar aerodynamics except for axial force where the AP09 shows only a small improvement in accuracy over the AP05.

Low-Drag Bomb Configurations

Five bomb configurations will be considered, four of which are from unlimited distribution documentation and one from limited

Table 7 Error comparisons of AP05 and AP09 aerodynamics to data for MK82 GPLDB

Based on Arnold Engineering Development Center data [24]							
M_∞	α	C_A errors, %		C_N errors, %		$X_{\text{c.p.}}/d$ errors, % of body length	
		AP05	AP09	AP05	AP09	AP05	AP09
0.6	0 deg	12.5	12.5	0.0	0.0	1.8	1.2
0.8	↓	6.1	6.1	↓	↓	2.9	0.8
0.9		13.1	13.1			2.0	1.2
1.1		1.1	1.1			1.1	0.7
1.3		9.3	9.3			0.6	0.2
1.5		11.5	11.5			8.9	3.0
0.6	8 deg	13.8	10.6	14.0	1.8	1.7	0.5
0.8	↓	10.0	1.2	6.7	3.3	1.2	1.1
0.9		14.5	14.6	4.4	2.9	0.4	3.3
1.1		1.9	1.9	7.5	7.5	1.9	3.1
1.3		17.8	17.8	1.5	0.0	2.4	2.0
1.5		9.7	15.8	20.7	22.4	3.7	1.1
0.6	16 deg	33.8	6.9	11.3	0.8	2.9	1.1
0.8	↓	31.1	12.0	2.1	2.1	0.2	2.1
0.9		46.1	46.2	3.7	12.4	2.9	4.1
1.1		4.2	4.2	6.4	5.1	6.1	4.9
1.3		15.1	15.1	10.6	10.0	5.1	3.9
1.5		11.1	0.6	7.9	10.8	1.4	3.3
0.6	24 deg	72.8	26.7	7.3	1.3	3.0	1.8
0.8	↓	60.0	26.5	2.7	3.1	1.2	2.9
0.9		46.6	46.9	9.4	4.9	3.2	4.4
1.1		0.5	0.5	2.4	2.0	4.8	4.5
1.3		21.6	21.6	8.7	8.1	3.1	2.6
1.5		31.7	15.9	5.3	8.4	0.5	3.9
Average		17.3	10.7	5.5	4.5	2.6	2.4
Based on Naval Ordnance Laboratory data [20]							
M_∞		C_{ℓ_p} errors, %		$C_{M_q} + C_{M_\dot{\alpha}}$ errors, %			
		AP05	AP09	AP05	AP09		
0.6		20.0	14.7	173.1	1.3		
0.8		21.3	13.3	180.0	38.7		
0.9		21.0	10.7	170.0	35.0		
1.1		39.0	1.7	45.3	28.0		
1.3		48.6	4.3	46.7	19.4		
1.5		64.7	14.7	44.3	24.5		
Average		35.8	9.9	109.9	24.5		

Table 8 Comparison of average static and dynamic aerodynamic prediction errors of the AP05 and AP09 compared with experiment for several bomb configurations

Bomb static aerodynamics summary									
Configuration	C_A errors, %		AP09 imp. over AP05, %	C_N errors, %		AP09 imp. over AP05, %	$X_{c.p.}/d$ errors, % of body length		AP09 imp. over AP05, %
	AP05	AP09		AP05	AP09		AP05	AP09	
1) MK82 GPLDB [20]	17.3	10.7	38.2	5.5	4.5	18.2	2.6	2.4	7.7
2) MK82 FF [23]	——	——	——	4.8	2.6	45.8	3.8	2.2	42.1
3) MK82 ISR [23]	——	——	——	10.0	11.4	−14.0	1.7	2.1	−23.5
4) MK82 ISRE [23]	——	——	——	8.5	7.1	16.5	1.9	3.5	−84.2
5) M117 [24]	12.0	12.0	0.0	4.0	4.0	0.0	3.8	2.8	26.3
				8.9	3.7	61.2			
Average	14.7	11.4	22.4	7.0	5.6	20.0	2.8	2.6	7.1

Bomb dynamic aerodynamics summary						
Configuration	C_{ℓ_p} errors, %		AP09 imp. over AP05, %	C_{M_q} errors, %		AP09 imp. over AP05, %
	AP05	AP09		AP05	APO9	
1) MK82 GPLDB [20]	35.8	9.9	72.3	109.9	24.5	77.7
2) MK82 FF [23]	21.3	8.3	61.0	36.6	16.2	55.7
3) MK82 ISR [23]	26.4	0.2	99.2	8.4	8.0	4.8
4) MK82 ISRE [23]	28.8	4.0	86.1	17.6	8.3	52.8
Average	28.1	5.6	80.1	43.1	14.3	66.8

distribution documentation. For the unlimited distribution configurations, plots of data and configurations can be shown along with the error analysis that is shown for limited distribution configurations. In addition to the five bomb configurations, one body–tail configuration with no boattail will be considered to illustrate the improvement in pitch damping that comes from excluding the portion of the body beneath the wing in body-alone pitch damping calculations, because the wing is assumed to extend to the body centerline for dynamic derivative calculations.

The first bomb configuration considered is the general purpose low-drag bomb (GPLDB), which is described in [20–24]. References [20–23] are unlimited distribution and [24] is limited distribution. The drawings of the configuration and charts of aerodynamics will therefore come from [20–23]. However, the aerodynamic error analysis of the static aerodynamics will come from [24]. Unfortunately, [24] was for static aerodynamics only, and so error comparisons for roll and pitch damping will be taken from [20,21].

Figure 9 shows the wind-tunnel model of [20], along with the AP09 approximation. The GPLDB is actually an ogive from the nose to a point midway back on the boattail where a straight conical section begins. The AP09 thus approximated the MK 82 GPLDB as a nose that extended up to approximately where the maximum diameter occurred, followed by an afterbody and a conical boattail. The boattail angle was selected to be identical to that on the GPLDB and thus the afterbody length was defined by the boattail angle and nose length.

Figures 10 and 11 show a comparison of the AP05 and AP09 C_N and $X_{c.p.}$ to experiment [20] at Mach numbers of 0.8, 1.56, and 2.16, and an AOA of 0–20 deg. Note the AP05 and AP09 normal-force coefficients are nearly identical, but the AP09 gives improved center of pressure prediction over the AP05 at all three Mach numbers considered. Figure 12 shows comparisons of pitch and roll damping between experiment and the AP05 and AP09 predictions. Note the significant improvement in dynamic derivative predictions of the AP09 over the AP05, and, in particular, the pitch damping predictions.

Table 7 now gives specific error comparisons of the AP05 and AP09 to full-scale static aerodynamic data of [24] and scaled wind-tunnel model dynamic derivative data of [20]. Note that the AP09 gives some slight improvement in all static aerodynamics (C_A, C_N, and $X_{c.p.}/d$) predictions compared with the AP05. Also note that both the AP05 and AP09 predictions of C_N and $X_{c.p.}/d$ are within the desired accuracy bounds of $\pm 10\%$ and $4\%\ \ell_B$, respectively. The final point to make from Table 7 is the large improvement in accuracy of roll and pitch damping of the AP09 compared with the AP05.

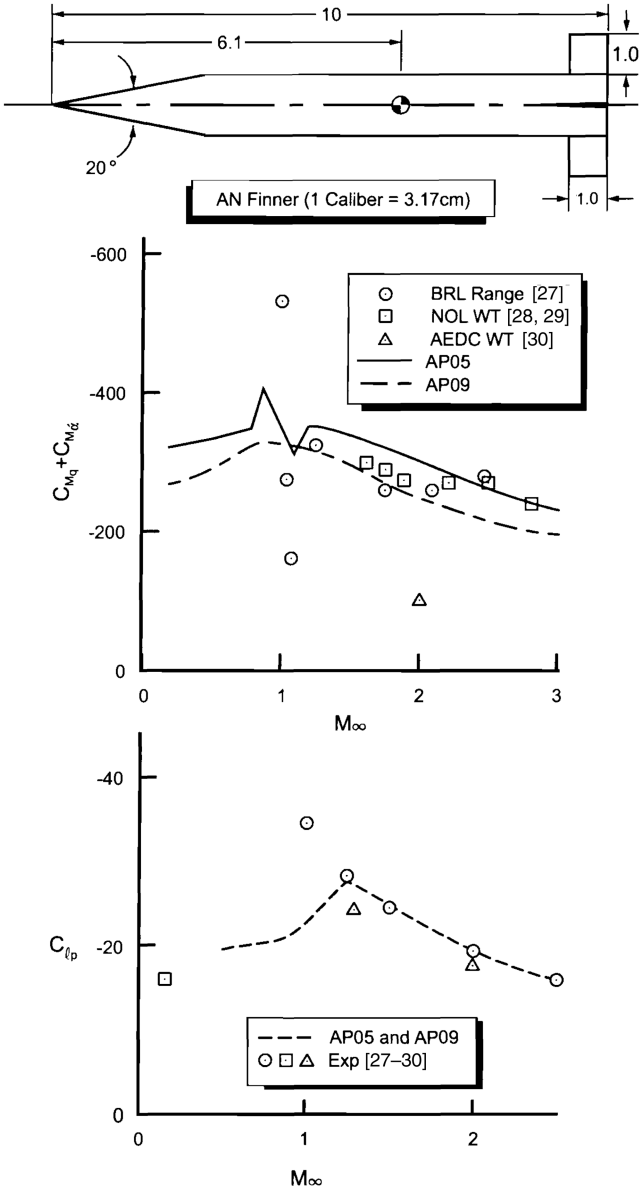

Fig. 13 Comparison of AP05 and AP09 dynamic derivatives to experiment for Army-Navy finner.

Table 8 now summarizes all the errors of the five bomb configurations. Only two cases have axial force data, and so the accuracy averages here are not as reliable due to a smaller sample. Also, only four of the five configurations had roll and pitch damping. Several points are worth making in viewing Table 8. First of all, the AP09 improves aerodynamic estimates of all static and dynamic predictions compared with the AP05. Errors of the AP09 are reduced by 22.4% for axial force, 20% for normal force, 7.1% for center of pressure, 80.1% for roll damping, and 66.8% for pitch damping when compared with the AP05. Second, both the AP05 and AP09 give average errors within the $\pm 10\%$ percent desired range for C_N and $\pm 4\%$ ℓ_B for $X_{\text{c.p.}}/d$. Third, the AP09 provides significant improvement in pitch and roll damping compared with the AP05.

The last configuration was considered to illustrate the error caused by not subtracting out the portion of body beneath the wings from the body-alone calculations. This error has been in all the versions of the Aeroprediction Code from the AP77 to the AP05. The case is the Army–Navy Finner (ANF). Many references (see [27–30]) are available that define the aerodynamics of the ANF. Figure 13 shows the ANF and the comparison of the pitch and roll damping AP05 and AP09 predictions compared with data. As seen in Fig. 13, there is no distinguishable difference in roll damping predictions of the AP05 and AP09 compared with data. This is because the body-alone roll damping is a small part of the total configuration damping. However, notice the improvement in pitch damping prediction of the AP09 compared with the AP05 for the ANF.

Summary

Several new or improved methods have been developed to improve the aerodynamic prediction accuracy of the Aeroprediction Code when applied to configurations with long boattails. In comparing the new methods to the AP05 predictions, it was seen the greatest improvement in predictions was for mortars with significant improvement also seen in low-drag bombs and projectiles. The greatest percent improvement in aerodynamics was for pitch damping, roll damping, center of pressure, and normal force, in that order, with only slight improvements in axial force. The new and improved methods will be part of the 2009 version of the Aeroprediction Code.

References

[1] Moore, F. G., and Hymer, T. C., "2005 Version of the Aeroprediction Code, Part 1: Summary of the New Theoretical Methodology," Aeroprediction Rept. No. 1, Jan. 2004.

[2] Moore, F. G., "*Approximate Methods for Weapon Aerodynamics*," Vol. 186, Progress in Astronautics and Aeronautics, AIAA, Reston, VA, Aug. 2000.

[3] Rogers, R. M., and Butler, C. B., "Aerodynamic Characteristics of Several Bluff Body Configurations at Subsonic and Transonic Mach Numbers," U.S. Air Force Advanced Technology Lab. TR-72-25, Feb. 1972.

[4] Wu, J. M., and Aoyoma, M., "Transonic Flow-Field Calculation Around Ogive Cylinders by Nonlinear-Linear Stretching Method," U.S. Army Missile Command, TR-RD-70-12, April 1970.

[5] Spring, D. J., "Effect of Nose Shape and Afterbody Length on the Normal Force and Neutral Point Location of Axisymmetric Bodies at Mach Numbers from 0.8 to 4.50," U.S. Army Missile Command Rept. No. RF-TR-64-13, 1964.

[6] Gwin, H., and Spring, D. J., "Stability Characteristics of a Family of Tangent Ogive-Cylinder Bodies at Mach Numbers 0.2 to 1.5," U.S. Army Missile Command Rept. No. RG-TR-61-1, 1961.

[7] Whyte, R. H., "Effects of Boattail Angle on Aerodynamic Characteristics of 175 mm M437 Projectile at Supersonic Mach Numbers," U.S. Army Munitions Command TM 1646, Sept. 1965.

[8] Washington, W. D., and Pettis, W., Jr., "Boattail Effects on Static Stability at Small Angles of Attack," U.S. Army Missile Command Rept. No. RD-TM-68-5, 1968.

[9] MacAllister, L. C., and Krial, K. S., "Aerodynamic Properties and Stability Behavior of the 155 mm Howitzer Shell M107," Ballistic Research Lab. Rept. No. 2547, Oct. 1975.

[10] Silton, S. I., "Navier–Stokes Computations for a Spinning Projectile from Subsonic to Supersonic Speeds," U.S. Air Force Research Lab. TR-2850, Sept. 2002.

[11] Chadwick, W. R., and Sylvester, J. F., "Dynamic Stability of the 5"/54 Rocket Assisted Projectile," U.S. Naval Weapons Lab. TR-2059, Oct. 1966.

[12] Ohlmeyer, E. J., "Dynamic Stability of the Improved 5"/54 Projectile," U.S. Naval Weapons Lab. TR-2871, Dec. 1974.

[13] Van Dyke, M. D., "First and Second-Order Theory of Supersonic Flow past Bodies of Revolution," *Journal of the Aeronautical Sciences*, Vol. 18, No. 3, March 1951, pp. 161–179.

[14] Moore, F. G., and Hymer, T. G., "Semiempirical Prediction of Pitch Damping Moments for Configurations with Flares," *Journal of Spacecraft and Rockets*, Vol. 38, No. 2, March–April 2001, pp. 150–158.

[15] Malejko, G., "Static Aerodynamics for the 120 MM XM984 Extended Range DPICM Mortar Projectile at Subsonic Mach Numbers," U.S. Army Armament Research, Development and Engineering Center, TR ARCCD-TR-00003, Jan. 2001.

[16] Owens, S., Dohrn, R., and Malejko, G., "Test 101 (LMHSWT 1419), High Speed Wind Tunnel Test, Precision Guided Mortar Munition (PGMM), Alliant Tech Systems Test Report," ATK Missile Systems Co., Rocket Center, WV, 20 April 2005.

[17] Owens, S., Dohrn, R., Sitts, J., and Malejko, G., "Test Report (Test 101B–Part 2) for the Precision Guided Mortar Munition (PGMM)," ATK Contractor Rept. prepared for U.S. Army Technical Agent Tank Automotive and Armaments, 2005.

[18] Malejko, G., "Effect of Fuze Windshield Separation on Flight Performance of the 60-MM, HE, M49A4 Projectile with Fuze, RD, M935," U.S. Army Armament Research, Development and Engineering Center, TR ARAED-TR-93009, Aug. 1993.

[19] Pierens, D. A., "Pitch and Roll Damping Coefficients of the Australian 81 mm Improved Mortar Projectile," Defense Science and Technology Organization TR-0020, May 1994.

[20] Piper, W. D., and DeMeritte, F. J., "Summary of the NOL Investigations to Date of the Aerodynamic Characteristics of the Navy Low Drag Bomb," Naval Ordnance Systems Command Rept. 5679, Feb. 1960.

[21] Schermerhorn, V. L., and DeMeriette, F. J., "Wind Tunnel Tests of the Navy Low-Drag Bomb at Angles of Attack up to 70 Degrees," Bureau of Naval Weapons Rept. 7291, March 1961.

[22] Krishnamoorthy, L. V., Kirk, D. R., and Glass, R., "Aerodynamic Data Base for the MK 82 General Purpose Low Drag Bomb," Defense Science and Technology Organization TR-0545, June 1997.

[23] Miklos, W. J., and Ingram, C. W., "Wind Tunnel Tests of three Candidate MK 82 Snakeye Bomb Replacement Configurations," U.S. Army Research Lab. Paper 75-0174, June 1975; National Technical Information Service AD-A014-735, U.S. Dept. of Commerce.

[24] Hobbs, R. W., "Drag Coefficient Table for a MK-82 LDGP Unguided Bomb Developed from Ground Based Techniques," Arnold Engineering Development Center TR-95-29, Feb. 1996.

[25] Falkowski, E. W., "Transonic Aerodynamic Characteristics of a Full-Scale M117 Bomb with Three Fin Configurations," U.S. Army Munitions Command TR 3785, Oct. 1968.

[26] Pierens, D., "Aerodynamic Evaluation of Production Fuzes and Fins for the 81 mm Improved Mortar Projectile," Defense Science and Technology Organization TR-0142, AR-008-331, March 1995.

[27] MacAllister, L. C., "Aerodynamic Properties of a Simple Non Rolling Finned Cone-Cylinder Configuration Between Mach Numbers 1.0 and 2.5," U.S. Army Ballistics Research Lab. Rept. No. 934, May 1955.

[28] Shantz, I., and Groves, R. T., "Dynamic and Static Stability Measurements of the Basic Finner at Supersonic Speeds," U.S. Naval Ordnance Lab. Rept. 4516, Sept. 1960.

[29] Regan, F. J., "Roll Damping Measurements of the Basic Finner at Subsonic and Supersonic Speeds," U.S. Naval Surface Warfare Center–Dahlgren Div. Rept. 6652, March 1964.

[30] Uselton, B. L., and Jenke, L. M., "Experimental Missile Pitch and Roll-Damping Characteristics at Large Angles of Attack," *Journal of Spacecraft and Rockets*, Vol. 14, No. 4, April 1977, pp. 241–247.

M. Miller
Associate Editor